

Unified Subharmonic Oscillation Conditions for Peak or Average Current Mode Control

Chung-Chieh Fang

Abstract

This paper is an extension of the author's recent research in which only buck converters were analyzed. Similar analysis can be equally applied to other types of converters. In this paper, a unified model is proposed for buck, boost, and buck-boost converters under peak or average current mode control to predict the occurrence of subharmonic oscillation. Based on the unified model, the associated stability conditions are derived in closed forms. The same stability condition can be applied to buck, boost, and buck-boost converters. Based on the closed-form conditions, the effects of various converter parameters including the compensator poles and zeros on the stability can be clearly seen, and these parameters can be consolidated into a few ones. High-order compensators such as type-II and PI compensators are considered. Some new plots are also proposed for design purpose to avoid the instability. The instability is found to be associated with large crossover frequency. A conservative stability condition, agreed with the past research, is derived. The effect of the voltage loop ripple on the instability is also analyzed.

Index Terms

current mode control, dc-dc power conversion, stability condition, subharmonic oscillation

arXiv:1310.7433v2 [cs.SY] 26 Jan 2014

CONTENTS

I	Nomenclature	2
II	Introduction	4
III	Review of FSI Conditions Based on Harmonic Balance Analysis	5
IV	Unified PCMC/ACMC Model for Different Converters	6
V	Applications to PCMC and ACMC	7
V-A	PCMC: Case \mathcal{C}_2	8
V-B	ACMC with Type-II Compensator: Case \mathcal{C}_5 or \mathcal{C}_9	9
V-B1	Based on SSAA: Converter is expected to be stable	9
V-B2	Based on HBA: FSI may occur even with $\text{PM} > 0$	9
V-C	ACMC with PI Compensator: Case \mathcal{C}_7 or \mathcal{C}_2	16
V-C1	Based on SSAA: Converter is expected to be stable	17
V-C2	Based on HBA: FSI may occur even with $\text{PM} \approx 90^\circ$	17
VI	The Effect of the Voltage Feedback Loop Ripple	20
VI-A	Proportional Gain Compensator: $G_v(s) = k_p$	22
VI-B	Type-II Compensator: $G_v(s) = K_c(1 + s/\omega_z)/s(1 + s/\omega_p)$	22
VI-C	PI Compensator: $G_v(s) = K_c(1/s + 1/\omega_z)$	23
VII	Conclusion and Contributions	23
	References	24

I. NOMENCLATURE

D	duty cycle (Note: dimensionless parameters are highlighted in red)
T	switching period
$f_s = 1/T$	switching frequency (unit: Hertz)
$\omega_s = 2\pi f_s$	angular switching frequency (unit: rad/s)
ω_c	crossover frequency
v_s	source (input) voltage
v_o	output voltage
v_r	reference voltage
v_c	control voltage (at the output of the voltage-loop compensator)
v_d	voltage across the diode
i_L	inductor current, a triangular wave in the time domain
$v_L = L(di_L/dt)$	voltage across the inductor, a square wave in the time domain
m_1	inductor current slope di_L/dt when the switch is on
$-m_2$	(negative) inductor current slope di_L/dt when the switch is off
$v_a = v_h - v_l$	amplitude of v_L (also note: $v_a = L(m_1 + m_2)$)
$v_h = Lm_1$	the high value of v_L
$v_l = -Lm_2$	the low value of v_L
$y(t)$	feedback signal for switching (the switch is turned off when $y \leq h$, for example)
$h(t)$	PWM or stabilizing ramp signal
V_h	the high value of the ramp
V_l	the low value of the ramp
$V_m = V_h - V_l$	ramp amplitude
$m_a = V_m/T = V_m f_s$	ramp slope
m_v	the effect on the required ramp slope m_a due to the (added) voltage loop ripple
L	inductance
C	capacitance
C_3	capacitance of a (ceramic) capacitor (with small ESR) in parallel with C
R	load resistance
R_s	sensing resistance (for the inductor current i_L)
R_c	equivalent series resistance (ESR) of C
$\rho = R/(R + R_c)$	a dimensionless parameter to show the effect of R_c ($\rho = 1$ if $R_c = 0$)
$\epsilon = \delta T$	switching delay

$\mathcal{T}(s) = \mathcal{T}_i(s) + \mathcal{T}_v(s)$	loop gain (with two parts contributed by the current and voltage loops)
$\mathcal{T}'(s) = e^{-s\epsilon}\mathcal{T}(s)$	loop gain with a switching delay $\epsilon := \delta T$
$\mathcal{T}_i(s)$	the part of loop gain contributed by the current loop
$\mathcal{T}_v(s)$	the part of loop gain contributed by the feedback voltage loop
C_1, C_2, C_3 , etc.	a case for a typical loop gain (see Table I or [4] for the case number)
K_c	compensator gain
ω_p	compensator pole
ω_z	compensator zero
$\omega_r = 1/R_c C$	ESR zero
$\omega_q = \omega_r(1 + C/C_3)$	a pole contributed by adding C_3 in parallel with C
$p = \omega_p/\omega_s$	normalized (by ω_s) compensator pole
$z = \omega_z/\omega_s$	normalized compensator zero
$r = \omega_r/\omega_s$	normalized ESR zero
$q = \omega_q/\omega_s$	normalized ω_q
$G_i(s) = R_s/sL$	current-loop integrator to convert v_L to $R_s i_L$ (for modeling purpose only)
$G_c(s)$	current-loop compensator transfer function
$G_v(s)$	voltage-loop compensator transfer function
$K = \frac{v_s R_s K_c}{V_m \omega_z L \omega_s}$	gain of the current feedback loop for the type-II compensator case
$K = Kz$	gain of the current feedback loop for the PI compensator case
K_{\max}	maximum allowable K to avoid subharmonic oscillation (i.e., need $K < K_{\max}$)
K_{\max}	maximum allowable K to avoid subharmonic oscillation (i.e., need $K < K_{\max}$)
$K_v = \frac{\rho v_s K_c}{TLC\omega_z}$	gain of the voltage feedback loop for the type-II compensator case
$k = \rho K_c T / R_s C \omega_z$	a dimensionless voltage feedback gain ($k = 0$ if the voltage feedback loop is open)
$\alpha(D, p)$	a function used as a building block of most typical stability conditions
$\alpha_k(D)$	the k -th coefficient term of $\alpha(D, p) = \sum_{k=0}^{\infty} (-1)^k \alpha_k(D) p^k$
$c(D, p)$	the high order $k \geq 2$ (correction) terms of $\alpha(D, p)$, i.e., $c(D, p) = \sum_{k=2}^{\infty} (-1)^k \alpha_k(D) p^k$
k_p	proportional feedback gain of the voltage loop
$\mathcal{F}(\mathcal{T}(s))$	an F-transform to convert a loop gain $\mathcal{T}(s)$ to a stability condition, $\mathcal{F}(\mathcal{T}(s)) < 1$
$\mathcal{S} = \mathcal{F}(m_a \mathcal{T}(s))$	an S-plot to show the required stabilizing ramp <i>slope</i> (stability requires $\mathcal{S} < m_a$)
$\mathcal{L} = \mathcal{F}(\mathcal{T}(s))$	an L-plot which is an F-transform of a <i>loop</i> gain (stability requires $\mathcal{L} = \mathcal{S}/m_a < 1$)
$m_i = \mathcal{F}(m_a \mathcal{T}_i(s))$	the part of the S-plot ($\mathcal{S} = m_i + m_v$) contributed by the current loop
$m_v = \mathcal{F}(m_a \mathcal{T}_v(s))$	the part of the S-plot contributed by the voltage feedback loop

II. INTRODUCTION

For DC-DC converters with current mode control (CMC) or voltage mode control (VMC), subharmonic oscillation (fast-scale instability, FSI) may occur [1], [2]. The instability is common in peak CMC (PCMC), but rarely reported in average CMC (ACMC) [3].

Consider the following four closely related nonlinear systems:

- \mathbb{S}_1 : a square wave generator (SWG) with a linear feedback;
- \mathbb{S}_2 : a buck converter;
- \mathbb{S}_3 : a triangular wave generator (TWG) with a linear feedback; and
- \mathbb{S}_4 : any CMC converter.

The systems \mathbb{S}_2 , \mathbb{S}_3 and \mathbb{S}_4 can be converted (denoted by “ \rightarrow ”) to \mathbb{S}_1 as shown below (see also Fig. 1):

$\mathbb{S}_2 \rightarrow \mathbb{S}_1$: In the buck converter, the voltage v_d across the diode (or the second switch) is a square wave, then $\mathbb{S}_2 \rightarrow \mathbb{S}_1$ [4], [5].

$\mathbb{S}_3 \rightarrow \mathbb{S}_1$: A TWG is equivalent to an SWG plus an integrator, and an integrator plus a linear feedback is still a linear feedback, then $\mathbb{S}_3 \rightarrow \mathbb{S}_1$.

$\mathbb{S}_4 \rightarrow \mathbb{S}_1$: In CMC, the inductor current i_L is a triangular wave (like an output of TWG), then $\mathbb{S}_4 \rightarrow \mathbb{S}_3 \rightarrow \mathbb{S}_1$, which makes a unified CMC model possible.

$\mathbb{S}_4 \rightarrow \mathbb{S}_1$: Also, the voltage $v_L = L(di_L/dt)$ across the inductor is a square wave, then $\mathbb{S}_4 \rightarrow \mathbb{S}_1$.

Although harmonic balance analysis (HBA) [4]–[6] has been applied to buck converters (\mathbb{S}_2 or \mathbb{S}_1) to obtain the FSI conditions, and experimentally verified in [7], its application to any CMC converter has not been reported. Based on the FSI conditions for \mathbb{S}_1 , this paper derives the general FSI conditions for \mathbb{S}_3 and \mathbb{S}_4 . As shown in Fig. 2, all of the results are independently verified by time-domain simulations and sampled-data analysis (SDA) [8], a known accurate analysis for DC-DC converters. FSI occurs when a sampled-data (discrete-time) pole crosses -1. The results are also compared with state-space average analysis (SSAA) which is less accurate.

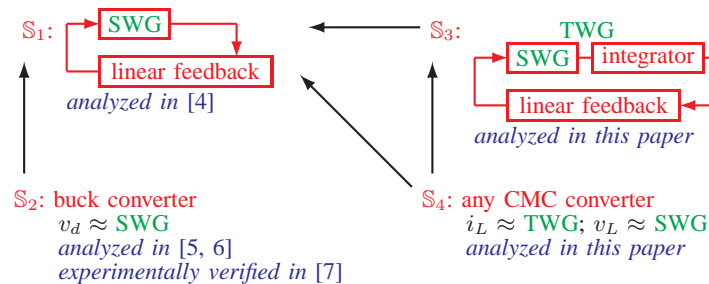


Figure 1. The systems \mathbb{S}_2 , \mathbb{S}_3 and \mathbb{S}_4 can be converted to \mathbb{S}_1 for further analysis.

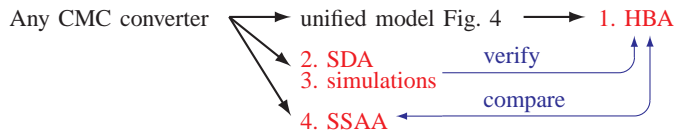


Figure 2. Throughout the paper, the CMC converter is analyzed in four ways: it is first analyzed by HBA, independently verified by SDA and simulations, and then compared with SSAA.

This paper focuses on the FSI conditions and tries to answer the following questions:

- 1) The buck and boost converters have different dynamics. For example, the boost converter has a right half plane zero [9]. Do these two converters with CMC essentially have the same dynamics?
- 2) In the past research [10] on PCMC, a sampling effect is included in order to predict FSI, which requires increasing the system dimension. However, its application to ACMC has been questioned [11], [12]. Also, the ramp in PCMC is used for stabilization, whereas the ramp in ACMC is used for PWM modulation. Does a unified CMC model, applicable to both PCMC and ACMC, exist without increasing the system dimension?
- 3) Is the unified CMC model also applicable to buck, boost, and buck-boost converters?
- 4) A converter has many parameters. Each parameter has a different effect. Can these parameters be consolidated into a few parameters to predict FSI? Is there a *single* plot which predicts FSI?

The answers to these questions will be shown to be affirmative.

For PCMC with open voltage loop, the FSI conditions have been well reported. For ACMC [3], [11]–[20], however, no accurate *general* closed-form FSI conditions have been reported. Also, the effects of the compensator poles and zeros on the stability have also not been reported. In this paper, the closed-form FSI conditions are derived, and the effects of many converter parameters can be clearly seen.

The remainder of the paper is organized as follows. The FSI conditions based on harmonic balance analysis [4] are reviewed in Section III. A unified CMC model is proposed in Section IV. It is then applied to various PCMC and ACMC schemes in Section V. The effect of the voltage loop ripple (at the output of the voltage-loop compensator) is considered in Section VI. Conclusions are collected in Section VII.

III. REVIEW OF FSI CONDITIONS BASED ON HARMONIC BALANCE ANALYSIS

FSI conditions based on harmonic balance analysis [4] are briefly reviewed. Consider a unity-gain SWG with a linear feedback. Denote the switching period as T and the switching frequency as $f_s = 1/T$, and let $\omega_s = 2\pi f_s$. Let the linear feedback transfer function be $\mathcal{T}(s)$. Let ω_p be the pole and ω_z be the zero,

Table I
STABILITY CONDITION FOR TYPICAL LOOP GAINS $\mathcal{T}(s)$ [4].

Case	$\mathcal{T}(s)$	Stability condition to avoid FSI
\mathcal{C}_1	$\frac{1}{s+\omega_p}$	$\frac{1}{\omega_s}\alpha(D, p) < 1$
\mathcal{C}_2	$\frac{1}{s}$	$\frac{1}{\omega_s}\alpha_0(D) < 1$
\mathcal{C}_5	$\frac{1}{s(1+s/\omega_p)}$	$\frac{1}{\omega_s}(\alpha_0(D) - \alpha(D, p)) < 1$
\mathcal{C}_7	$\frac{1+s/\omega_z}{s^2}$	$\frac{1}{\omega_s^2}(\frac{1}{z}\alpha_0(D) + \alpha_1(D)) < 1$
\mathcal{C}_9	$\frac{1+s/\omega_z}{s^2(1+s/\omega_p)}$	$\frac{1}{\omega_s^2}(\alpha_1(D) + (\frac{1}{p} - \frac{1}{z})(\alpha(D, p) - \alpha_0(D))) < 1$

for example. Let $p = \omega_p/\omega_s$ and $z = \omega_z/\omega_s$. Let D be the duty cycle. Take $\mathcal{T}(s) = \omega_s/(s + \omega_p)$, for example. The stability condition (to avoid FSI) is $\alpha(D, p) < 1$, where

$$\begin{aligned}
\alpha(D, p) &= 2\pi c \operatorname{sch}(2\pi p) - \pi e^{\pi p(1-2D)} \operatorname{csch}(\pi p) \\
&:= \sum_{k=0}^{\infty} (-1)^k \alpha_k(D) p^k \\
&:= \alpha_0(D) - \alpha_1(D)p + c(D, p) \\
\alpha_0(D) &= \pi(2D - 1) \\
\alpha_1(D) &= \pi^2(2D^2 - 2D + 1)
\end{aligned}$$

For other typical loop gains [4], see Table I. Based on partial fraction decomposition of $\mathcal{T}(s)$, most FSI conditions are related with $\alpha(D, p)$, which is a building block of other FSI conditions [4]. It is also the reason why a special form of $\alpha(D, p)$ is defined as above.

IV. UNIFIED PCMC/ACMC MODEL FOR DIFFERENT CONVERTERS

Consider a CMC boost converter shown in Fig. 3, where $G_c(s)$ is the current-loop compensator transfer function, $G_v(s)$ is the voltage-loop compensator transfer function, v_s is the source voltage, v_o is the output voltage, v_c is the control voltage, v_r is the reference voltage, R_s is sensing resistance, y is a feedback signal, and h is a PWM or compensating ramp varying from V_l to V_h . In Sections IV and V, v_c is assumed constant. The effect of voltage loop ripple is analyzed in Section VI. Let the equivalent series resistance (ESR) be R_c . Denote the ramp slope as m_a and the ramp amplitude as $V_m = V_h - V_l = m_a T$.

The inductor current i_L is a triangular wave, and the voltage across the inductor $v_L(t) = L di_L/dt$ is a square wave. Therefore, a CMC converter can be represented by a *unified* model shown in Fig. 4. Let the square wave $v_L(t)$ have a high value v_h , a low value v_l , and an amplitude $v_a = v_h - v_l$, as shown in Fig. 5 for different converters. Take the boost converter, for example. When the switch is on, $L di_L/dt = v_s$. When the switch is off, $L di_L/dt = v_s - v_o$. Then, $v_a = v_s - (v_s - v_o) = v_o = v_s/(1 - D)$. Denote

Table II

UNIFIED STABILITY CONDITIONS (IN TERMS OF RAMP SLOPE m_a) FOR DIFFERENT CMC SCHEMES, APPLICABLE TO ANY CMC CONVERTER.

PCMC	$\mathcal{S} := \frac{v_a R_s}{L} (D - \frac{1}{2}) < m_a$
ACMC (type-II)	$\mathcal{S} := \frac{v_a R_s K_c}{T L \omega_s^2} ((\alpha_1(D) + (\frac{1}{p} - \frac{1}{z})(\alpha(D, p) - \alpha_0(D)))) < m_a$
(for $\omega_z \ll \omega_s$)	$\mathcal{S} := \frac{v_a R_s K_c}{T \omega_z L \omega_s} (\alpha_0(D) - \alpha(D, p)) < m_a$
(for $\omega_z \ll \omega_s$)	$K := \frac{v_a R_s K_c}{V_m \omega_z L \omega_s} < K_{\max}(D, p) := \frac{1}{\alpha_0(D) - \alpha(D, p)}$
ACMC (PI)	$\mathcal{S} := \frac{v_a R_s K_c}{L} (\frac{2D-1}{2\omega_z} + \frac{(1-2D+2D^2)T}{4}) < m_a$
	$K := \frac{v_a R_s K_c}{V_m L \omega_s^2} < K_{\max}(D, z) := \frac{1}{\alpha_0(D)/z + \alpha_1(D)}$

Note: $v_a = v_s$ for buck converters and $v_a = v_s/(1 - D)$ for boost or buck-boost converters.

Table III

STABLE/UNSTABLE BOOST CONVERTERS IN EXAMPLES 1-3.

Ex.	K or K	D	p or z	Stability	In parameter space	Simulation	PM
1	$K = 0.4$	0.86	$p = 0.75$	unstable	[a] in Figs. 7(d) & 6(d)	Fig. 8	60°
	$K = 0.4$	0.85	$p = 0.75$	stable	[b] in Fig. 7(d)	Fig. 10	
2	$K = 1.3$	0.36	$p = 0.17$	stable	[c] in Fig. 7(c)	Fig. 11	
	$K = 1.3$	0.36	$p = 0.18$	unstable	[d] in Figs. 7(c) & 6(c)	Fig. 12	18°
	$K = 1.3$	0.36	$p = 0.515$	unstable	[e] in Figs. 7(c) & 6(c)	Fig. 14	33°
	$K = 1.3$	0.36	$p = 0.52$	stable	[f] in Fig. 7(c)	Fig. 16	
3	$K = 0.0232$	0.6	$z = 0.018$	unstable	[g] in Figs. 19(c) & 23	Fig. 20	89°
	$K = 0.0232$	0.58	$z = 0.018$	stable	[h] in Figs. 19(c) & 23	Fig. 22	

A. PCMC: Case \mathcal{C}_2

In PCMC, $y = v_c - R_s i_L$, $G_c(s) = 1$ and $\mathcal{T}(s) = v_a G_i(s)/V_m = v_a R_s/sV_m L$ which belongs to case \mathcal{C}_2 . Let \mathcal{S} be an S-plot [4] to show the required stabilizing ramp slope. For $\mathcal{S} < m_a$, the converter is stable. From Table I, the stability condition is

$$\frac{v_a R_s \alpha_0(D)}{V_m L \omega_s} < 1 \quad \text{or} \quad \mathcal{S} := \frac{v_a R_s (D - 0.5)}{L} < m_a \quad (1)$$

where $v_a = v_s$ for buck converters and $v_a = v_s/(1 - D)$ for boost or buck-boost converters, agreed with [21].

B. ACMC with Type-II Compensator: Case \mathcal{C}_5 or \mathcal{C}_9

For ACMC, $y = G_c(s)(v_c - R_s i_L) + v_c$, which has an additional offset v_c but does not affect the loop gain. Let the type-II phase-lead compensator (with $\omega_z < \omega_p$) be

$$G_c(s) = \frac{K_c(1 + s/\omega_z)}{s(1 + s/\omega_p)} \quad (2)$$

where K_c is a gain. Generally, $\omega_z \ll \omega_s$. Let $K = v_a R_s K_c / V_m \omega_z L \omega_s$. Then

$$\mathcal{T}(s) = \frac{v_a G_c(s) G_i(s)}{V_m} = \frac{v_a R_s K_c (1 + \frac{s}{\omega_z})}{V_m L s^2 (1 + \frac{s}{\omega_p})} \quad (3)$$

$$\approx \frac{K \omega_s}{s(1 + \frac{s}{\omega_p})} \quad (\text{at frequency } \omega_s \gg \omega_z) \quad (4)$$

1) *Based on SSAA: Converter is expected to be stable:* Let ω_c be the crossover frequency. Setting $|\mathcal{T}(j\omega_c)| = 1$ in (4) leads to

$$\omega_c = \frac{\omega_s}{\sqrt{2}} \sqrt{\sqrt{p^4 + 4K^2 p^2} - p^2} \quad (5)$$

$$\approx \begin{cases} \omega_s K & (\text{for } K \ll p) \\ \omega_s \sqrt{Kp} & (\text{for } K \gg p) \end{cases} \quad (6)$$

A large K leads to a large ω_c . From (4), the phase margin (PM) is $90^\circ - \arctan(\omega_c/\omega_p) > 0$. PM is a function of K and p , independent of D . For $K = 100, 2, 1.3$, and 0.4 , the plots of PM in the (D, p) space are shown in Fig. 6, and the converter is expected to be always stable. As K decreases, ω_c decreases and PM increases.

2) *Based on HBA: FSI may occur even with PM > 0:* From (4), $\mathcal{T}(s)$ belongs to case \mathcal{C}_5 in Table I, and the stability condition to avoid FSI is

$$K(\alpha_0(D) - \alpha(D, p)) < 1 \quad (7)$$

which can be expressed in terms of the required ramp slope m_a , as shown in Table II. FSI may occur if (7) is not met. For the same K as in Fig. 6, the stable regions according to (7) are shown in Fig. 7. As K decreases, the stability region enlarges, but there still exist instability regions. From [5], no subharmonic oscillation occurs if $K < 1/\pi$, which is a conservative condition and it is approximately equivalent to $\omega_c < \omega_s/\pi$ according to (6). A large ω_c leads to FSI. However, such a condition $\omega_c < \omega_s/\pi$ may be too conservative. The converter can be designed according to the limit (7) with larger ω_c for higher performance without losing stability.

Note that PM in Fig. 6 is independent of D , whereas the stability in Fig. 7 depends on D . Comparing Fig. 7 with Fig. 6, one sees that the converter may be unstable even with PM = 60° , for example, if $K = 0.4$, $D = 0.86$, and $p = 0.75$ as shown in the next example.

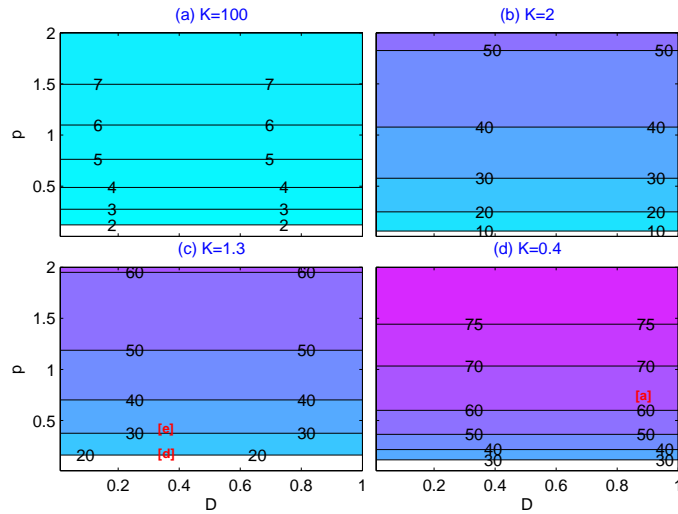


Figure 6. As K decreases, PM increases, independent of D , but FSI still occurs as shown in Fig. 7, different colors for different PM.

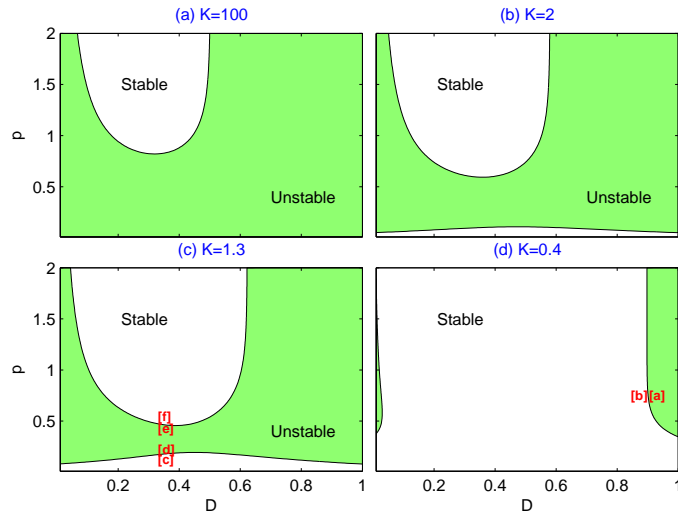


Figure 7. As K decreases, the instability region still exists but shrinks.

Example 1. (FSI with $PM = 60^\circ$.) Consider an ACMC boost converter (adapted from the *buck* converter in [5]) with a type-II compensator: $v_o = 14$ V, $V_m = 1$ V, $f_s = 50$ kHz, $L = 46.1$ μ H, $C = 380$ μ F, $R_c = 0.02$ Ω , $R_s = 16.4$ m Ω , $R = 1$ Ω , $\omega_z = 5652.9$ rad/s, $p = 0.75$, $K_c = 141670$, and $K = 0.4$.

First, let $v_s = 1.96$ V and $v_c = 1.64$ V. Here, $D = 0.86$. The converter is unstable (Fig. 8) although its average model has $PM = 60^\circ$ (Fig. 9). The linear average model is too simple to predict the FSI of the nonlinear converter. Independent sampled-data analysis also shows an unstable pole at -1.02 , and three stable poles at 0 , 0.88 , and 0.91 , thus verifying the instability.

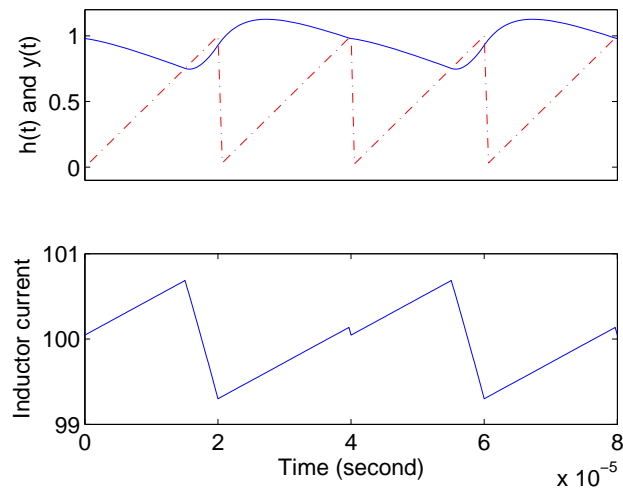


Figure 8. The boost converter is unstable, $v_s = 1.96$ V.

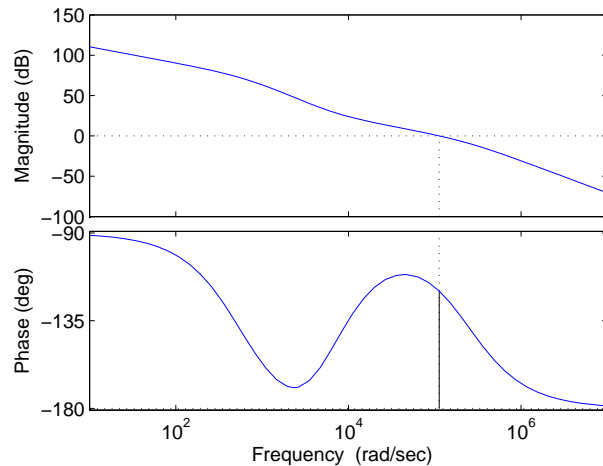


Figure 9. The loop gain $\mathcal{T}(j\omega)$ has $\text{PM} = 60^\circ$, $v_s = 1.96$ V.

Next, let $v_s = 2.1$ V and $v_c = 1.53$ V. Now, $D = 0.85$. The converter is stable (Fig. 10). In Fig. 7(d), for $K = 0.4$, draw a line at $p = 0.75$. The instability occurs indeed around $D = 0.86$. \square

As reported in [5], the *ACMC buck* converter may have an unstable *window* of p . The next example shows that the *boost* converter also has the same unstable window.

Example 2. (Unstable window of p in the boost converter, adapted from the buck converter in [5].) Continue from Example 1, but with $v_s = 9$ V, $v_c = 0.357$ V, and $K_c = 460420$. This *boost* converter example is actually adapted from Example 3 of [5] for a *buck* converter, where an unstable window of p

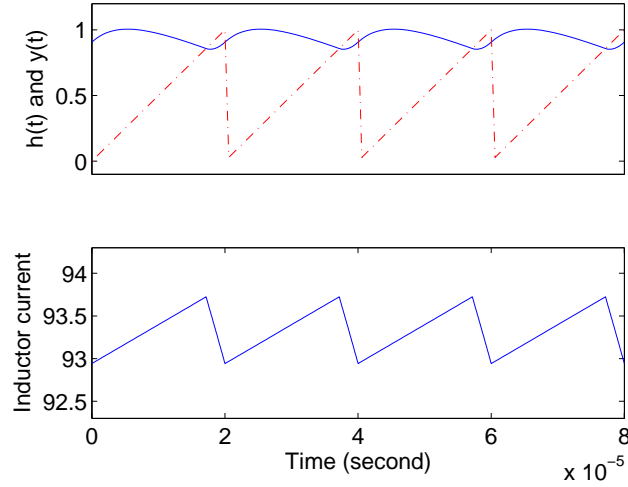


Figure 10. The boost converter is stable, $v_s = 2.1$ V.

was found. This example also illustrates the buck and boost converters, known to have different dynamics, have the same occurrence of FSI with the same parameters. Both examples have the same $v_a = 14$ V, where $v_a = v_s$ for the buck converter and $v_a = v_o$ for the boost converter. Both examples also have the same $D = 0.36$ and $K = 1.3$ (and also other parameters such as R , L , C , R_c , and ω_z). Therefore, an unstable window of p for this boost converter is also expected. In Fig. 7(c), for $K = 1.3$, draw a line at $D = 0.36$, which shows an unstable window of $p \in [0.18, 0.515]$. For $p < 0.18$ or $p > 0.515$, the converter is stable.

First, let $p = 0.17$. The converter is stable (Fig. 11).

Second, let $p = 0.18$. The converter is unstable (Fig. 12) although its average model has $\text{PM} = 18^\circ$ (Fig. 13). Independent sampled-data analysis shows an unstable pole at -1.07 , and three stable poles at 0.35 , 0.88 , and 0.91 .

Third, let $p = 0.515$. The converter is unstable (Fig. 14) although its average model has $\text{PM} = 33^\circ$ (Fig. 15). Independent sampled-data analysis shows an unstable pole at -1.002 , and three stable poles at -0.05 , 0.88 , and 0.91 .

Fourth, let $p = 0.52$. The converter is stable again (Fig. 16). The boost converter indeed has an unstable window of $p \in [0.18, 0.515]$, same as the buck converter in [5]. \square

Note that $K = v_a R_s K_c / V_m \omega_z L \omega_s$, and one can see the effect of each parameter on the stability. The condition (7) can be expressed in terms of the required ramp slope m_a , as shown in Table II:

$$m_a > \mathcal{S} := \frac{v_o R_s K_c}{2\pi \omega_z L} (\alpha_0(D) - \alpha(D, p)) \quad (8)$$

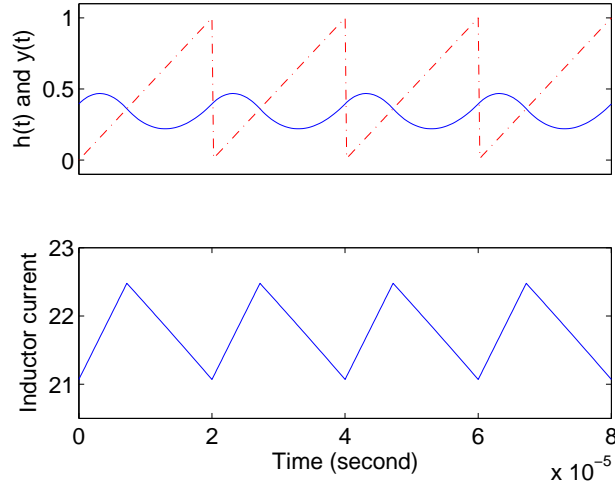


Figure 11. The boost converter is stable, $p = 0.17$.

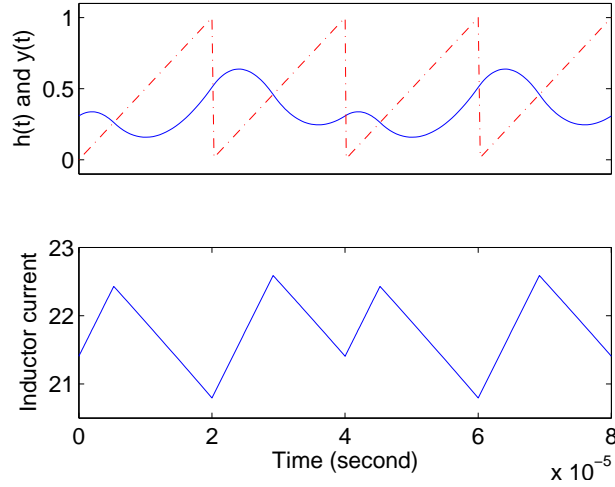


Figure 12. The boost converter is unstable, $p = 0.18$.

The condition (7) can be also expressed in terms of K :

$$K < \frac{1}{\alpha_0(D) - \alpha(D, p)} := K_{\max}(D, p) \quad (9)$$

if $K_{\max}(D, p)$ is positive. If $K_{\max}(D, p)$ is negative, the converter is always stable (because the inequality sign in (9) is reversed and the condition (9) is always met).

For the *boost* converter, $v_a = v_o$ which is fixed (if regulated), and (9) becomes

$$K = \frac{v_o R_s K_c}{V_m \omega_z L \omega_s} < K_{\max}(D, p) \quad (10)$$

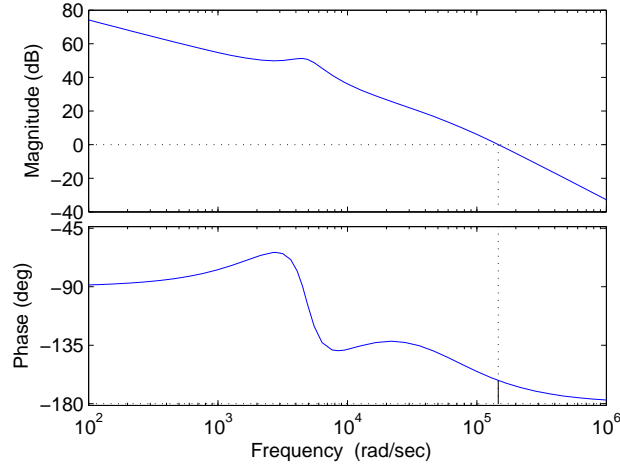


Figure 13. The loop gain $\mathcal{T}(j\omega)$ has $PM = 18^\circ$, $p = 0.18$.

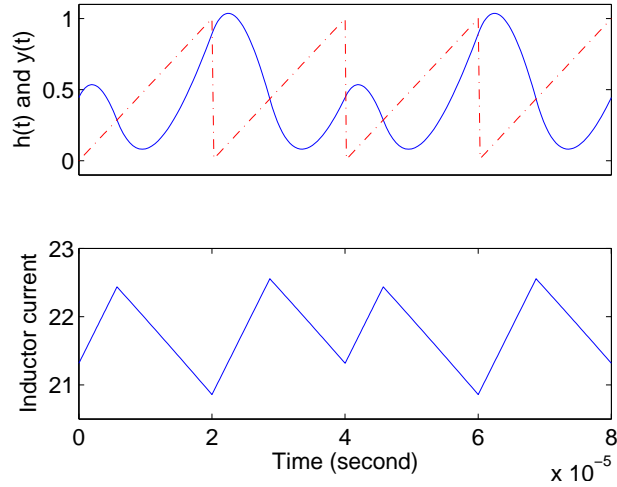


Figure 14. The boost converter is unstable, $p = 0.515$.

In [11, Eq. 14], a conservative condition was proposed:

$$\frac{v_o R_s K_c}{V_m \omega_z L \omega_s} < \min\left[\frac{1}{\pi(1-D)}, \frac{1}{2\pi}\right] = \frac{1}{2\pi} \quad (11)$$

where the effect of p was neglected. The plots of (11) and $K_{\max}(D, p)$ for different values of p are shown in Fig. 17.

The plot of $K_{\max}(D, p)$ is quite nonlinear. As p increases from 0.1 to 0.3, $K_{\max}(D, p)$ decreases, whereas as p increases from 0.4 to 0.7 (and beyond), $K_{\max}(D, p)$ increases. It indicates that around $p = 0.3$ the stability region shrinks, agreed with Fig. 7 which also indicates a possible unstable window

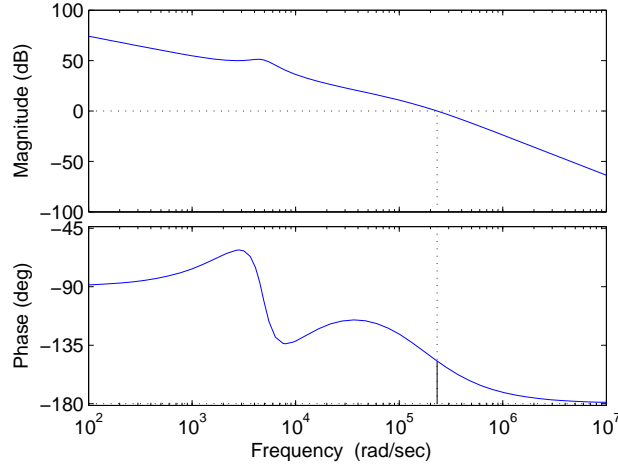


Figure 15. The loop gain $\mathcal{T}(j\omega)$ has $PM = 33^\circ$, $p = 0.515$.

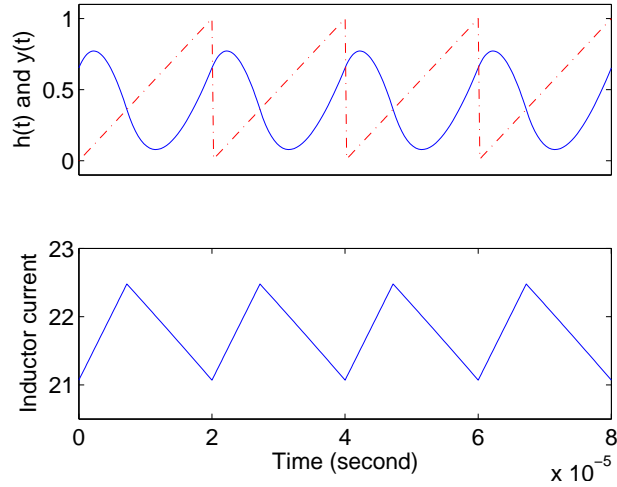


Figure 16. The boost converter is stable, $p = 0.52$.

of p . One sees that the condition (11) reported in [11] is conservative because $K_{\max}(D, p) > 1/2\pi$ as shown in Fig. 17.

As indicated in Fig. 17, the converter is prone to be stable around $D = 0.4$ (than other values of D), also agreed with Fig. 7. The closed-form $K_{\max}(D, p)$ is such nonlinear that it is difficult to further simplify it. Instead, one can make the plot of $K_{\max}(D, p)$ to predict the stability.

Since a *single* $K = v_a R_s K_c / V_m \omega_z L \omega_s$ contains *many* design parameters, the plot of $K_{\max}(D, p)$ is very useful to design a stable converter. Given the values of p and the ranges of D , one can make a plot of $K_{\max}(D, p)$ and adjust different parameters so that the condition $K < K_{\max}(D, p)$ is met.

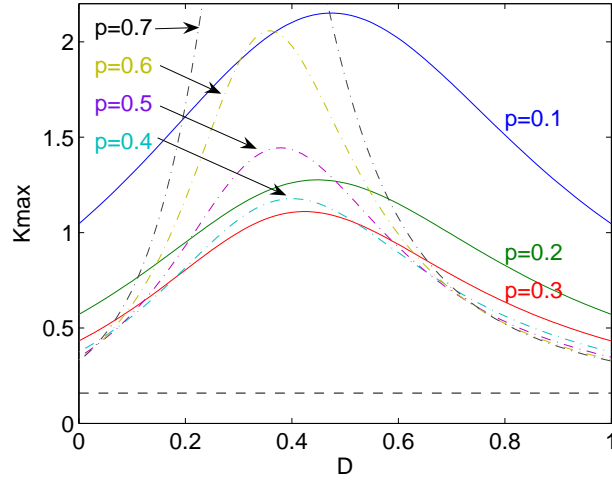


Figure 17. The plots of $K_{\max}(D, p)$ for the boost converter, dashed line for the conservative condition (11).

For the *buck* converter, $v_a = v_s = v_o/D$ and (9) becomes

$$\frac{v_o R_s K_c}{V_m \omega_z L \omega_s} < D K_{\max}(D, p) \quad (12)$$

In [11, Eq. 13], a conservative condition was proposed:

$$\frac{v_o R_s K_c}{V_m \omega_z L \omega_s} < \min\left[\frac{D}{\pi(1-D)}, \frac{1}{2\pi}\right] \quad (13)$$

The plots of (13) and $D K_{\max}(D, p)$ for different values of p are shown in Fig. 18. As p increases from 0.1 to 0.3, $D K_{\max}(D, p)$ decreases. As p increases from 0.4 to 0.7, $D K_{\max}(D, p)$ increases. One sees that the condition (13) reported in [11] is also conservative. From Fig. 18, the buck converter is susceptible to FSI if D is too small.

In the above analysis, $\omega_z \ll \omega_s$ is assumed. If that is not the case, the loop gain (3) belongs to case \mathcal{C}_9 . Based on Table I, the (general) stability condition is

$$\mathcal{S} := \frac{v_a R_s K_c}{T L \omega_s^2} \left((\alpha_1(D) + \left(\frac{1}{p} - \frac{1}{z}\right)(\alpha(D, p) - \alpha_0(D))) \right) < m_a \quad (14)$$

C. ACMC with PI Compensator: Case \mathcal{C}_7 or \mathcal{C}_2

Let the PI compensator be

$$G_c(s) = \frac{K_c(1 + s/\omega_z)}{s} \quad (15)$$

Although the PI compensator is a special case of the type-II compensator by setting $\omega_p \rightarrow \infty$ in (2), here $\omega_z \ll \omega_s$ is not assumed as in Sec. V-B and a separate discussion on the effect of ω_z is needed.

Let $K = v_a R_s K_c / V_m L \omega_s^2$ (a little different from K). Then

$$\mathcal{T}(s) = \frac{v_a G_c(s) G_i(s)}{V_m} = \frac{v_a R_s K_c (1 + \frac{s}{\omega_z})}{V_m L s^2} = \frac{K \omega_s^2 (1 + \frac{s}{\omega_z})}{s^2} \quad (16)$$

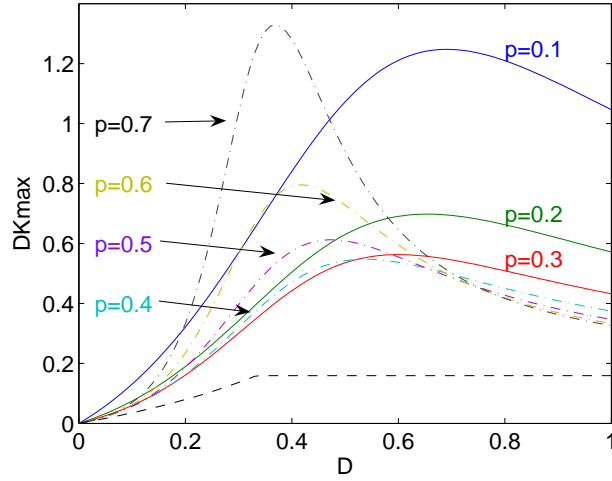


Figure 18. The plots of $DK_{\max}(D, p)$ for the buck converter, dashed line for the conservative condition (13).

1) *Based on SSAA: Converter is expected to be stable:* Setting $|\mathcal{T}(j\omega_c)| = 1$ in (16) leads to

$$\omega_c = \frac{\sqrt{2}\omega_s K z}{\sqrt{\sqrt{K^4 + 4K^2 z^4} - K^2}} \quad (17)$$

For $z^2 \ll K$, $\omega_c \approx \omega_s K/z$ and $\text{PM} = \arctan(\omega_c/\omega_z) = \arctan(K/z^2) \approx 90^\circ$. However, FSI may still occur as discussed next.

2) *Based on HBA: FSI may occur even with $\text{PM} \approx 90^\circ$:* From (16), $\mathcal{T}(s)$ belongs to case \mathcal{C}_7 in Table I, and the stability condition is

$$K\left(\frac{\alpha_0(D)}{z} + \alpha_1(D)\right) < 1 \quad (18)$$

Express (18) in terms of the required ramp slope m_a , as shown in Table II:

$$m_a > \mathcal{S} := \frac{v_a R_s K_c}{4L\omega_z} (4D - 2 + (1 - 2D + 2D^2)T\omega_z) \quad (19)$$

For $T\omega_z \ll 1$ (generally true), the stability condition (19) becomes

$$m_a > \mathcal{S} := \frac{v_a R_s K_c}{L\omega_z} \left(D - \frac{1}{2}\right) \quad (20)$$

agreed with [3, Eq. 9]. For $D < 1/2$, the converter is stable even if $m_a = 0$. For $D > 1/2$, a ramp slope with (20) is required. A small ω_z also makes the loop gain (16) belong to \mathcal{C}_2 (which has a stability condition like PCMC) instead of \mathcal{C}_7 . Setting $D = 1$ in (20), a (conservative) ramp slope $m_a = v_a R_s K_c / 2L\omega_z$ stabilizes the converter for any D .

For $K = 0.2, 0.05, 0.02$, and 0.002 , the stable regions are shown in Fig. 19. For $K < 0.002$, the whole region in Fig. 19 is almost stable. However, FSI still occurs for $D > 0.5$ if z is too small. From Fig. 19, the stability is z dependent, even for small $z < 0.1$.

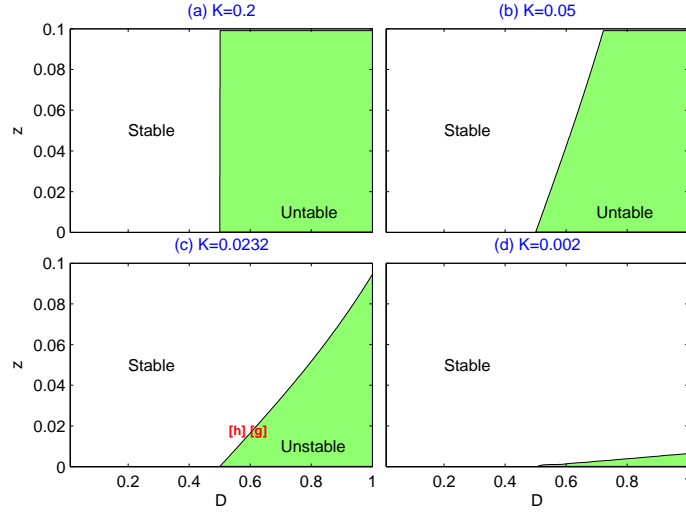


Figure 19. As K decreases or z increases, the stability region enlarges.

Example 3. (FSI with $PM = 89^\circ$.) Continue from Example 1, but with large $\omega_p = 3.14 \times 10^9$ rad/s (to make the type-II compensator act like a PI compensator), $v_s = 5.6$ V, $v_c = 0.574$ V, and $K_c = 460420$. Here, $z = 0.018$, $D = 0.6$ and $K = 0.0232$. The converter is unstable (Fig. 20) although its average model has $PM = 89^\circ$ (Fig. 21). Independent sampled-data analysis shows an unstable pole at -1.02 , and three stable poles at 0 , 0.88 , and 0.91 .

Next, let $v_s = 5.88$ V and $v_c = 0.547$ V. Now, $D = 0.58$. The converter is stable (Fig. 22). In Fig. 19(c), for $K = 0.02$, draw a line at $z = 0.018$, and the instability indeed occurs around $D = 0.6$.

□

The condition (18) can be also expressed in terms of K :

$$K < \frac{1}{\alpha_0(D)/z + \alpha_1(D)} := K_{\max}(D, z) \quad (21)$$

if $\alpha_0(D)/z + \alpha_1(D)$ is positive.

For the boost converter, $v_a = v_o$, and (21) becomes

$$K = \frac{v_o R_s K_c}{V_m L \omega_s^2} < K_{\max}(D, z) \quad (22)$$

The plots of $K_{\max}(D, z)$ for different values of z are shown in Fig. 23. For $D < 1/2$, the converter is stable, agreed with Fig. 19. If z is small, the converter is prone to be unstable for $D > 0.5$, agreed with (20). As z increases, $K_{\max}(D, z)$ increases and the stability region enlarges, also agreed with Fig. 19. The plots of $K_{\max}(D, z)$ also agree with Example 3. Draw a line at $K = 0.0232$ in Fig. 23, the line intersects with $K_{\max}(D, 0.018)$ around $D = 0.6$ indicating the onset of FSI at $D = 0.6$ as discussed in Example 3.

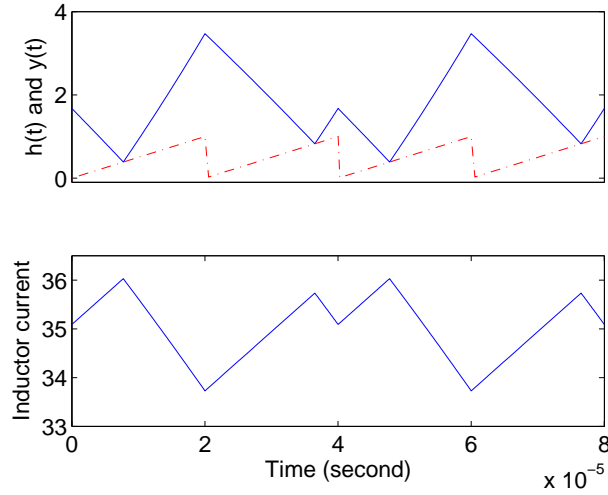


Figure 20. The boost converter is unstable, $v_s = 5.6$ V.

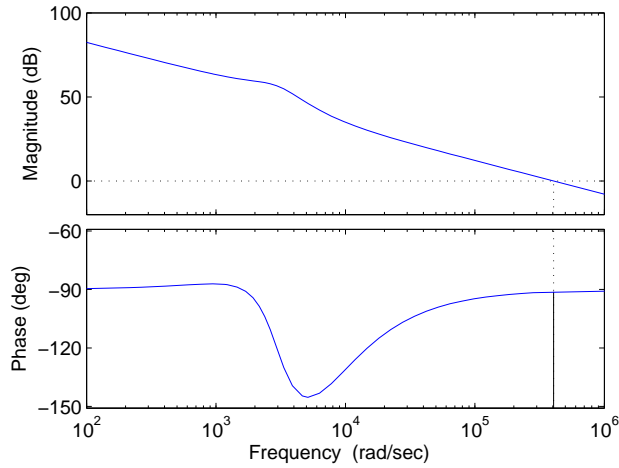


Figure 21. The loop gain $\mathcal{T}(j\omega)$ has PM = 89°, $v_s = 5.6$ V.

In Fig. 23, given any value of z , $K_{\max}(D, z)$ has a minimum at $D = 1$. Then, a conservative (valid for any D) stability condition is

$$K < K_{\max}(1, z) = \frac{z}{\pi(1 + \pi z)} < \frac{z}{\pi} \quad (23)$$

As discussed above, $\omega_c \approx \omega_s K/z$ for $z^2 \ll K$. Then, (23) is equivalent to $\omega_c < \omega_s/\pi$. This agrees with the tradition wisdom not to set a large ω_c to avoid FSI [5]. In Examples 1-3, FSI occurs with $\omega_c > \omega_s/\pi$.

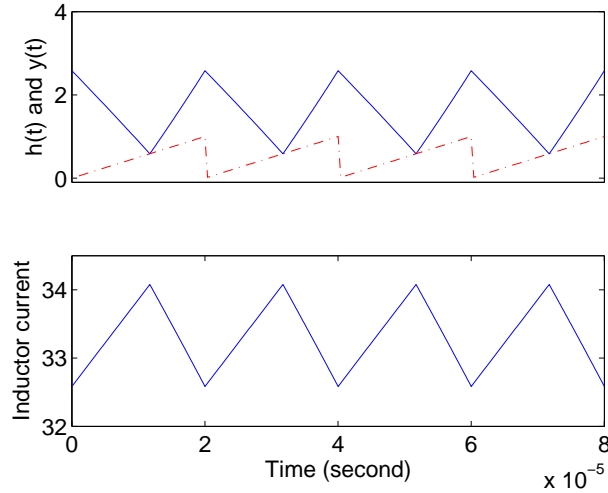


Figure 22. The boost converter is stable, $v_s = 5.88$ V.

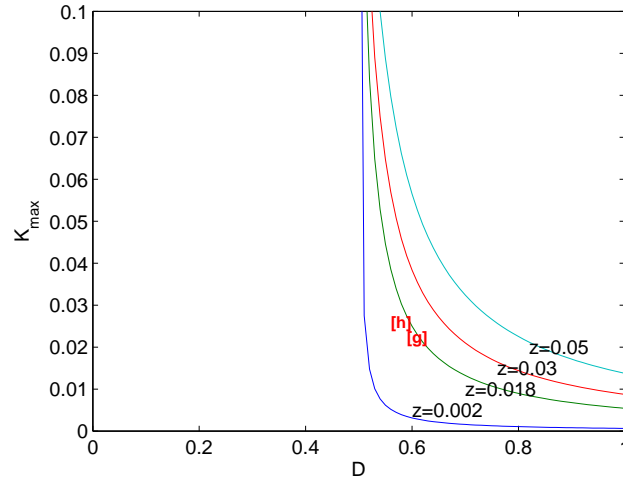


Figure 23. The plots of $K_{\max}(D, z)$ for the boost converter.

VI. THE EFFECT OF THE VOLTAGE FEEDBACK LOOP RIPPLE

In the above analysis, v_c is assumed constant. In this section, the effect of v_c ripple generated from the voltage feedback loop is analyzed. Consider the PCMC buck converter, for example. Similar analysis can be applied to the ACMC case.

For PCMC, $G_c(s) = 1$ and $y = v_c - R_s i_L$ which has two terms, for the voltage and current loops, respectively. Let (the ESR zero) $\omega_r = 1/R_c C$, $r = \omega_r/\omega_s$ and $\rho = R/(R + R_c)$. Let $G(s) := -y(s)/v_L(s)$.

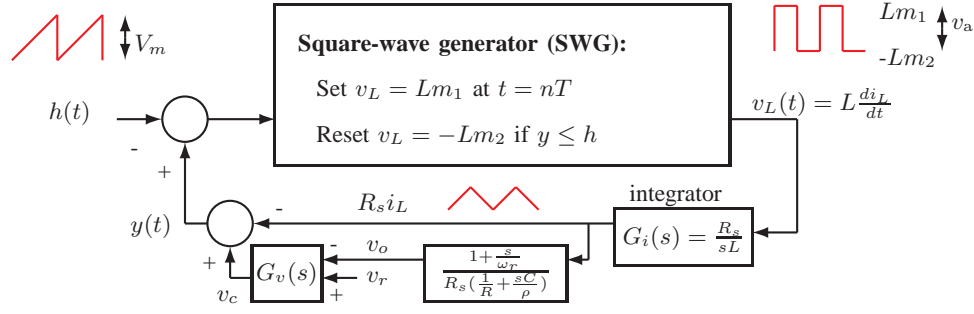


Figure 24. A model for PCMC buck converter with closed voltage loop.

Table IV

STABILITY CONDITIONS FOR PCMC BUCK CONVERTER WITH OPEN OR CLOSED VOLTAGE LOOP.

Universal stability condition:	$\frac{v_s R_s (D - 0.5)}{L} < m_a - m_v$
Voltage loop open:	$m_v = 0$
Voltage loop closed:	
Proportional gain compensator, $G_v(s) = k_p$:	$m_v = \frac{\rho v_s k_p}{TLC\omega_s^2} [\frac{1}{r}\alpha_0(D) + \alpha_1(D)]$
Type-II compensator, $G_v(s) = \frac{K_c(1+s/\omega_z)}{s(1+s/\omega_p)}$:	$m_v = \frac{K_v}{\omega_s^2} [\alpha_1(D) + (\frac{1}{p} - \frac{1}{r})(\alpha(D, p) - \alpha_0(D))]$
PI compensator, $G_v(s) = \frac{K_c(1+s/\omega_z)}{s}$:	$m_v = \frac{K_v}{\omega_s^2} [\frac{1}{r}\alpha_0(D) + \alpha_1(D)]$
Note: $p = \omega_p/\omega_s$, $z = \omega_z/\omega_s$, $r = \omega_r/\omega_s = 1/R_c C\omega_s$, $\rho = R/(R + R_c)$, and $K_v = \rho v_s K_c / TLC\omega_z$	

For the buck converter,

$$\frac{v_o(s)}{i_L(s)} = R \parallel (R_c + \frac{1}{sC}) = \frac{1 + \frac{s}{\omega_r}}{\frac{1}{R} + \frac{sC}{\rho}} \approx \frac{\rho(1 + \frac{s}{\omega_r})}{sC} \quad (\text{at high frequency}) \quad (24)$$

Based on Fig. 4 and as shown in Fig. 24, the PCMC buck converter can be modeled as an SWG plus $G(s)$, where

$$G(s) = (1 + \frac{\rho(1 + s/\omega_r)G_v(s)}{R_s C s^2})G_i(s) \quad (25)$$

The loop gain is

$$\mathcal{T}(s) = \frac{v_a G(s)}{V_m} = \frac{v_s G(s)}{V_m} \approx \frac{v_s R_s}{V_m L s} + \frac{\rho v_s (1 + s/\omega_r) G_v(s)}{V_m L C s^2} \quad (26)$$

Three different voltage-loop compensators (with different $G_v(s)$) are considered. The stability conditions have a *universal* form, $v_s R_s (D - 0.5)/L < m_a - m_v$, even if different voltage-loop compensators are used, and those stability conditions are summarized in Table IV.

A. *Proportional Gain Compensator*: $G_v(s) = k_p$

Let the voltage feedback be $v_c = k_p(v_r - v_o)$. From (26),

$$\mathcal{T}(s) = \frac{v_s R_s}{V_m L s} + \frac{\rho v_s k_p (1 + s/\omega_r)}{V_m L C s^2} \quad (27)$$

From Table I, the stability condition is

$$\frac{v_s R_s \alpha_0(D)}{V_m L \omega_s} + \frac{\rho v_s k_p}{V_m L C \omega_s^2} \left(\frac{1}{r} \alpha_0(D) + \alpha_1(D) \right) < 1 \quad (28)$$

or expressed in terms of the ramp slope

$$\frac{v_s R_s (D - 0.5)}{L} < m_a - m_v \quad (29)$$

where, compared with (1), the (universal) stability condition (29) has an additional term

$$m_v = \frac{\rho v_s k_p}{T L C \omega_s^2} \left[\frac{1}{r} \alpha_0(D) + \alpha_1(D) \right] \quad (30)$$

due to the effect of the voltage loop ripple. Note that $\alpha_1(D) > 0$, but $\alpha_0(D) < 0$ if $D < 0.5$. Depending on whether m_v is positive or negative, the stability region shrinks or enlarges respectively by closing the voltage loop. It can be proved that for most practical buck converters, $m_v > 0$.

The stability condition (28) can be also expressed in terms of k_p ,

$$k_p < \frac{\frac{\omega_s C}{\rho} (V_m L \omega_s - R_s \alpha_0(D))}{\frac{1}{r} \alpha_0(D) + \alpha_1(D)} \quad (31)$$

Example 4. (Accurate prediction of critical gain k_p^ .)* Consider a PCMC buck converter with the voltage loop closed from Example 4 of [1]. Simulation and independent sampled-data analysis show that FSI occurs at $k_p^* = 237$ (see Fig. 7 of [1]), which can be predicted by (31) exactly. In contrary, with $k_p = 237$, the Ridley average model [10] shows that the converter is stable with an infinite gain margin and PM = 36.5° [1]. \square

B. *Type-II Compensator*: $G_v(s) = K_c(1 + s/\omega_z)/s(1 + s/\omega_p)$

Let the voltage feedback be $v_c = G_v(s)(v_r - v_o) + v_r$, which has an additional offset v_r but it does not affect the loop gain. From (26), the loop gain is

$$\mathcal{T}(s) = \frac{v_s R_s}{V_m L s} + \frac{\rho v_s K_c (1 + s/\omega_r)(1 + s/\omega_z)}{V_m L C s^3 (1 + s/\omega_p)} \quad (32)$$

Generally $\omega_z \ll \omega_s$. Let $K_v = \rho v_s K_c / T L C \omega_z$. From Table I, the stability condition is also (29), where

$$m_v = \frac{K_v}{\omega_s^2} \left[\alpha_1(D) + \left(\frac{1}{p} - \frac{1}{r} \right) (\alpha(D, p) - \alpha_0(D)) \right] \quad (33)$$

C. *PI Compensator*: $G_v(s) = K_c(1/s + 1/\omega_z)$

The PI compensator is a special case of the type-II compensator by setting $\omega_p \rightarrow \infty$. Let the control voltage at the output of the voltage-loop compensator be $v_c = G_v(s)(v_r - v_o) + v_r$. From (26), the loop gain is

$$\mathcal{T}(s) = \frac{v_s R_s}{V_m L s} + \frac{\rho v_s K_c (1 + s/\omega_r)(1 + s/\omega_z)}{V_m L C s^3} \quad (34)$$

Generally $\omega_z \ll \omega_s$. From Table I, the stability condition is also (29), where

$$m_v = \frac{K_v}{\omega_s^2} \left[\frac{1}{r} \alpha_0(D) + \alpha_1(D) \right] \quad (35)$$

Note that (35) is for the PI compensator whereas (30) is for the proportional compensator. However, they are the same by setting $k_p = K_c/\omega_z$. The proportional compensator, though simple, can be used to predict FSI if a more complicated PI compensator is used.

VII. CONCLUSION AND CONTRIBUTIONS

Based on [4], [5], a unified CMC model (Fig. 4) is proposed to predict FSI for different converters under PCMC or ACMC. Such a unified CMC model exists because any CMC converter is essentially a TWG with a linear feedback. Closed-form stability conditions are derived (see Table II) and verified by time-domain simulations (see Table III). The obtained results are consistent with (but broader than) the past research such as [3], [11]. The instability is found to be associated with large crossover frequency. A conservative condition to avoid FSI is $\omega_c < \omega_s/\pi$. The proposed model can be applied to converters with high-order compensators, such as type-II and PI compensators, for example.

The questions asked in the Introduction are answered:

- 1) FSI occurs in both the buck and the boost converters with the same parameters if they have the same v_a , as shown in Example 2.
- 2) The *unified* model can be applied to both PCMC and ACMC.
- 3) The *same* FSI condition expressed in terms of v_a , as shown in Table II, also applies to any CMC converter. For the buck converter, $v_a = v_s = v_o/D$. For the boost or buck-boost converter, $v_a = v_s/(1 - D) = v_o$. For example, given a buck converter with $v_o = v_a D$ and a boost converter with $v_o = v_a$, if both of the converters have the same power stage parameters, then they have the same stability or instability.
- 4) Although different parameters have different effects, they can be consolidated into a few parameters: K , D , and p . A *single* plot of $K_{\max}(D, p)$ can be used to predict FSI. The stability based on traditional average analysis is D independent (Fig. 6), whereas the actual stability is D dependent (Fig. 7).

To the author's knowledge, the following contributions have not been reported:

- 1) The *unified* CMC model of Fig. 4, applicable to PCMC or ACMC buck, boost, and buck-boost converters.
- 2) The *unified* stability conditions in Table II.
- 3) The plots of Figs. 6, 7, 17-19, and 23, which are *universal* for any CMC converter, and they are not just for specific examples.
- 4) Using the plot of $K_{\max}(D, p)$ as a design tool to avoid FSI.
- 5) The effects of different parameters on the stability, such as K , the compensator pole ω_p and zero ω_z , as shown in Figs. 7 and 19.
- 6) The conservative stability condition $\omega_c < \omega_s/\pi$ for the CMC converter with a *PI* compensator (whereas the same condition for the CMC converter with the *type-II* compensator was reported in [5]).
- 7) The effect of the voltage loop ripple on FSI (see Table IV).

Although this paper focuses on CMC, the proposed analysis can be applied to other schemes (such as VMC and constant on-time control). As reported in [5], ACMC with type-II and PI compensators belong respectively to the cases \mathcal{C}_5 and \mathcal{C}_7 . The derived FSI conditions are also applicable to these cases. For example, a buck converter with V^2 control belongs to the case \mathcal{C}_7 with $K = v_s/V_m LC\omega_s^2$ and $\omega_z = 1/R_c C$, and the stability condition is exactly (18). Also, a buck converter with a type-II, type-III, or phase-lead compensator belongs to the case \mathcal{C}_5 , and the stability condition is exactly (7).

REFERENCES

- [1] C.-C. Fang. Sampled-data poles, zeros, and modeling for current mode control. *Int. J. of Circuit Theory Appl.*, 41(2):111–127, Feb. 2013.
- [2] Y. Chen, C. K. M. Tse, S. Qiu, L. Lindenmuller, and W. Schwarz. Coexisting fast-scale and slow-scale instability in current-mode controlled DC/DC converters: Analysis, simulation and experimental results. *IEEE transactions on circuits and systems I, Regular papers*, 55(10):3335–3348, Nov. 2008.
- [3] T. Suntio, J. Lempinen, I. Gadoura, and K. Zenger. Dynamic effects of inductor current ripple in average current mode control. In *Proc. IEEE PESC*, pages 1259–1264, 2001.
- [4] C.-C. Fang. Critical conditions for a class of switched linear systems based on harmonic balance: Applications to dc-dc converters. *Nonlinear Dynamics*, 70(3):1767–1789, Nov. 2012.
- [5] C.-C. Fang. Closed-form critical conditions of subharmonic oscillations for buck converters. *IEEE Trans. Circuits Syst. I*, 60(7):1967–1974, Jul. 2013.
- [6] C.-C. Fang. Closed-form critical conditions of instabilities for constant on-time controlled buck converters. *IEEE Trans. Circuits Syst. I*, 59(12):3090–3097, Dec. 2012.
- [7] C.-C. Fang and R. Redl. Subharmonic stability limits for the buck converter with ripple-based constant on-time control and feedback filter. *IEEE Trans. Power Electron.*, 29(4):2135–2142, Apr. 2014.

- [8] C.-C. Fang and E. H. Abed. Saddle-node bifurcation and Neimark bifurcation in PWM DC-DC converters. In S. Banerjee and G. C. Verghese, editors, *Nonlinear Phenomena in Power Electronics: Bifurcations, Chaos, Control, and Applications*, pages 229–240. Wiley, New York, 2001.
- [9] R. W. Erickson and D. Maksimovic. *Fundamentals of Power Electronics*. Springer, Berlin, Germany, second edition, 2001.
- [10] R. B. Ridley. A new, continuous-time model for current-mode control. *IEEE Trans. Power Electron.*, 6(2):271–280, 1991.
- [11] J. Sun and R. M. Bass. Modeling and practical design issues for average current control. In *Proc. IEEE APEC*, pages 980–986, 1999.
- [12] Y. Yan, F.C. Lee, and P. Mattavelli. Analysis and design of average current mode control using describing function-based equivalent circuit model. *IEEE Trans. Power Electron.*, 28(10):4732–4741, Oct. 2013.
- [13] L. H. Dixon. Average current-mode control of switching power supplies. *Unitrode Power Supply Design Seminar Handbook*, 1990.
- [14] W. Tang, F. C. Lee, and R. B. Ridley. Small-signal modeling of average current-mode control. *IEEE Trans. Power Electron.*, 8(2):112–119, Apr. 1993.
- [15] C. Sun, B. Lehman, and R. Ciprian. Dynamic modeling and control in average current mode controlled PWM DC/DC converter. In *Proc. IEEE PESC*, pages 1152–1157, 1999.
- [16] P. Cooke. Modeling average current mode control. In *Proc. IEEE APEC*, pages 256–262, 2000.
- [17] R. Li. Modeling average-current-mode-controlled multi-phase buck converters. In *Proc. IEEE APEC*, pages 3299–3305, Aug. 2008.
- [18] R. Li, T. O’Brien, J. Lee, and J. Beecroft. A unified small signal analysis of DC-DC converters with average current mode control. In *Proc. IEEE ECCE*, pages 647–654, 2009.
- [19] R. Li, T. O’Brien, J. Lee, and J. Beecroft. Effects of circuit and operating parameters on the small-signal dynamics of average-current-mode-controlled DC-DC converters. In *IEEE 8th International Conference on Power Electronics and ECCE Asia*, pages 60–67, 2011.
- [20] F. Yu, F.C. Lee, and P. Mattavelli. A small signal model for average current mode control based on describing function approach. In *Proc. IEEE ECCE*, pages 405–412, 2011.
- [21] C.-C. Fang. Asymmetric critical conditions for peak and valley current programmed converters at light loading. *IEEE Transactions on Circuits and Systems-I: Regular Papers*, 2013. accepted, available: <http://dx.doi.org/10.1109/TCSI.2013.2284178>.